A R C H I V E O F M E C H A N I C A L E N G I N E E R I N G

VOL. LXIII 2016 Number 4

DOI: 10.1515/meceng-2016-0031

**Key words:** bone remodelling, artificial disc, lumbar spine, FE analysis

*PAWEŁ WYMYSŁOWSKI*,[1] *TOMASZ ZAGRAJEK*[1]

# BONE REMODELLING MODEL INCORPORATING BOTH SHAPE AND INTERNAL STRUCTURE CHANGES BY THREE DIFFERENT RECONSTRUCTION MECHANISMS. A LUMBAR SPINE CASE

The paper presents a method of analysis of bone remodelling in the vicinity of implants. The authors aimed at building a model and numerical procedures which may be used as a tool in the prosthesis design process. The model proposed by the authors is based on the theory of adaptive elasticity and the lazy zone concept. It takes into consideration not only changes of the internal structure of the tissue (described by apparent density) but also surface remodelling and changes caused by the effects revealing some features of "creep". Finite element analysis of a lumbar spinal segment with an artificial intervertebral disc was performed by means of the Ansys system with custom APDL code. The algorithms were in two variants: the so-called site-independent and site-specific. Resultant density distribution and modified shape of the vertebra are compared for both of them. It is shown that this two approaches predict the bone remodelling in different ways. A comparison with available clinical outcomes is also presented and similarities to the numerical results are pointed out.

## 1. Introduction

Bone is not formed once for its whole life but undergoes constant changes as other living tissues. Continuous processes of removing of old bone (bone resorption) and creation of new one (ossification) take place. These processes are called bone remodelling and last with different intensity throughout the whole life. Ossification dominates in childhood and youth up to 30 years of age when the peak bone mass is achieved, whereas bone resorption prevails in later stages of life. General shape of the skeleton is gene-dependant but the final mass and structure results from many factors, biological (nutrition, medicines etc.) as well as mechanical.

[1] *Institute of Aeronautics and Applied Mechanics, Warsaw University of Technologu, Nowowiejska 24, 00-665 Warsaw; Emails: pwymyslo@meil.pw.edu.pl, tzagra@meil.pw.edu.pl*

They can change microstructure (internal remodelling) or even shape of bone (external remodelling) if the existing equilibrium is disturbed [1]. Remodelling, which is a response to mechanical loading of bone, is called the functional adaptation [2]. The issue is crucial in implantation: inserting a prosthesis into the bone system leads to a change in load distribution and finally to the above-mentioned process.

Many contemporary models of the phenomenon are based on the Cowin's theory of adaptive elasticity [3]. Usually, they focus on changes in internal structure of the bone tissue only, and neglect the change of shape [4]. Taking into account some kind of the external remodelling is rare [5] and sometimes applies to the trabecular level [6]. The main goal of this work was to create a model which can simulate both these factors (i.e. the change of internal structure and the shape of bone) and may be used as a tool in the prosthesis design process.

## 2. Material and methods

### 2.1. Model of functional adaptation

The model developed by the authors is also based on the Cowin's theory of adaptive elasticity and the concept of "lazy range" of the stimulus (strain energy density), but it takes into consideration simultaneous changes in internal structure (described by apparent density) and shape of the bone. It assumes that bone is a continuous isotropic tissue of two kinds: trabecular and cortical. The structure, and therefore mechanical properties of the bone, are changed by a mechanical stimulus (specific strain energy defined as strain energy density divided by apparent density). The apparent density is related to the Young's modulus by the known equation:

$$E = \alpha \rho^{\beta} \tag{1}$$

where $E$ is Young's modulus [MPa], $\rho$ apparent density [g/cm$^3$] , $\alpha$ and $\beta$ are experimental factors.

The model incorporates three mechanisms:

1. change in thickness of cortical bone,
2. change in apparent density,
3. "creep-like" behaviour of bone [7].

#### 2.1.1. Change in thickness of cortical bone

It is assumed that the change in thickness is the primary mechanism of remodelling for cortical bone. For the stimulus values within the lazy zone (homeostatic equilibrium), the thickness remains unchanged, whereas for higher values it increases and for lower values it decreases (Fig. 1a). Additionally, for very high as well for very low stimuli, the mechanism is turned off in favour of the change in

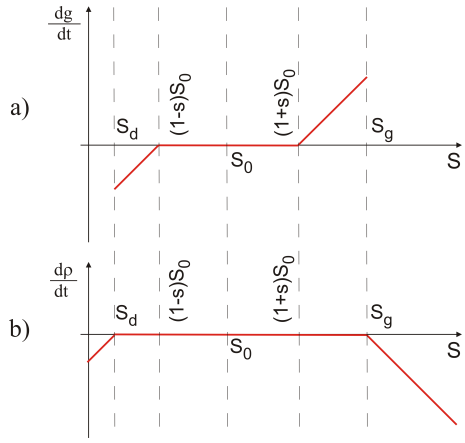


Fig. 1. Rate of change in thickness (a) and rate of change in density (b) of cortical bone.

density, because it is believed that the latter can better describe sudden atrophy of bone. According to this assumptions, the rate of change in thickness is written as:

$$\frac{\mathrm{d}g}{\mathrm{d}t} = \begin{cases} 0 & \text{for} \quad S \leqslant S_d \\ Ae^{-A_1 t}\left[S - (1-s)\,S_0\right] & \text{for} \quad S_d < S \leqslant (1-s)\,S_0 \\ 0 & \text{for} \quad (1-s)\,S_0 < S < (1+s)\,S_0 \\ Ae^{-A_1 t}\left[S - (1+s)\,S_0\right] & \text{for} \quad (1+s)\,S_0 \leqslant S < S_g \\ 0 & \text{for} \quad S_g \leqslant S \end{cases} \tag{2}$$

where: $S_0$, $s$ – parameters describing lazy zone of cortical zone, $S_d$, $S_g$ – lower and upper values of stimulus which limit the zone of changes of thickness, $A$, $A_1$ – experimental factors.

### 2.1.2. Change of apparent density

The rate of change in density is calculated differently for cortical and trabecular bone. For the former one, the mechanism is activated if underloading or overloading takes place and leads to a reduction in the apparent density (sudden bone atrophy) in both cases (Fig. 1b):

$$\frac{\mathrm{d}\rho}{\mathrm{d}t} = \begin{cases} Ce^{-C_1 t}\,(S - S_d) & \text{for} \quad S \leqslant S_d \\ -Ce^{-C_1 t}\left(S - S_g\right) & \text{for} \quad S_g \leqslant S \end{cases} \tag{3}$$

For trabecular bone, the mechanism is assumed to be primary and only one. It causes a decrease in the density for the stimulus lower than the lazy zone, an increase in the density for the stimulus higher than that, and again a decrease for big overloading. The stimulus within the lazy zone means that no changes are

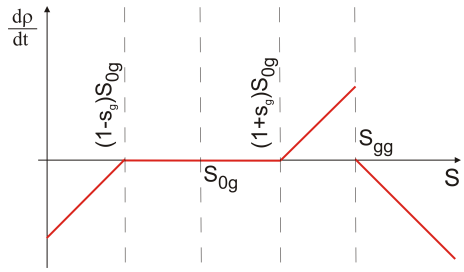


Fig. 2. Rate of change in apparent density of trabecular bone

observed (Fig. 2). This relations are written as:

$$\frac{\mathrm{d}\rho}{\mathrm{d}t} = \begin{cases} C_g e^{-C_{1g}t}\left[S - \left(1 - s_g\right) S_{0g}\right] & \text{for} \quad S < \left(1 - s_g\right) S_{0g} \\ 0 & \text{for} \quad \left(1 - s_g\right) S_{0g} \leqslant S \leqslant \left(1 + s_g\right) S_{0g} \\ C_g e^{-C_{1g}t}\left[S - \left(1 + s_g\right) S_{0g}\right] & \text{for} \quad \left(1 + s_g\right) S_{0g} < S \leqslant S_{gg} \\ -C_g e^{-C_{1g}t}\left(S - S_{gg}\right) & \text{for} \quad S_{gg} < S \end{cases} \tag{4}$$

The parameters in the above formulae are: $S_{0g}$, $s_g$ – parameters describing lazy zone of trabecular bone, $S_{gg}$ – superior limit of stimulus, if the stimulus exceeds the value the bone is destroyed, $C$, $C_1$, $C_g$, $C_{1g}$ – experimental factors.

### 2.1.3. "Creep-like" behaviour

Change of shape („creep-like" behaviour) described by permanent displacement $u_p$ is expressed by the formula:

$$u_p = Be^{-B_1 t}\mathbf{u}_f \tag{5}$$

where: $\mathbf{u}_f$ – displacement caused by the load, $B$, $B_1$ – experimental factors.

### 2.1.4. Site specific formulation

The values of parameters which describe lazy zones and drive the remodelling processes ($S_0$, $s$, $S_{0g}$, $s_g$, $S_{gg}$, $S_d$, $S_g$) may be formulated as site-independent (equal at every point of the bone) or site-specific (different values at different points of the bone). In the latter case, the parameters depend on load level of healthy bone with no prosthesis implanted.

For site-specific formulation, it is more convenient to use another, normalized, description of the rates of changes. The rate of change in thickness formula (2) may

be rewritten as:

$$\frac{\mathrm{d}g}{\mathrm{d}t} = \begin{cases} 0 & \text{for} \quad S \leqslant S_d \\ A_L e^{-A_{1L}t}\left[\dfrac{S}{S_0} - (1-s)\right] & \text{for} \quad S_d < S \leqslant (1-s)\,S_0 \\ 0 & \text{for} \quad (1-s)\,S_0 < S < (1+s)\,S_0 \\ A_L e^{-A_{1L}t}\left[\dfrac{S}{S_0} - (1+s)\right] & \text{for} \quad (1+s)\,S_0 \leqslant S < S_g \\ 0 & \text{for} \quad S_g \leqslant S \end{cases} \tag{6}$$

Instead of the formula of the rate of change in density, for cortical bone (3) the following formula is used:

$$\frac{\mathrm{d}\rho}{\mathrm{d}t} = \begin{cases} C_L e^{-C_{1L}t}\left(\dfrac{S}{S_0} - \dfrac{S_d}{S_0}\right) & \text{for} \quad S \leqslant S_d \\ -C_L e^{-C_{1L}t}\left(\dfrac{S}{S_0} - \dfrac{S_g}{S_0}\right) & \text{for} \quad S_g \leqslant S \end{cases} \tag{7}$$

Finally, the formula for the trabecular bone (4) is changed into:

$$\frac{\mathrm{d}\rho}{\mathrm{d}t} = \begin{cases} C_{gL} e^{-C_{1gL}t}\left[\dfrac{S}{S_{0g}} - \left(1-s_g\right)\right] & \text{for} \quad S < \left(1-s_g\right) S_{0g} \\ 0 & \text{for} \quad \left(1-s_g\right) S_{0g} \leqslant S \leqslant \left(1+s_g\right) S_{0g} \\ C_{gL} e^{-C_{1gL}t}\left[\dfrac{S}{S_{0g}} - \left(1+s_g\right)\right] & \text{for} \quad \left(1+s_g\right) S_{0g} < S \leqslant S_{gg} \\ -C_{gL} e^{-C_{1gL}t}\left(\dfrac{S}{S_{0g}} - \dfrac{S_{gg}}{S_{0g}}\right) & \text{for} \quad S_{gg} < S \end{cases} \tag{8}$$

The parameters $A_L$, $A_{1L}$, $C_L$, $C_{1L}$, $C_{gL}$, $C_{1gL}$ are experimental factors analogous to those in expressions (2), (3) and (4).

### 2.2. Numerical formulation

Numerical procedure of the remodelling model uses finite element method and proceeds according to the block diagram illustrated in Fig. 3.

The analysis of changes in the bone over the time is conducted in steps $i$. Every step is described by time parameter $t_i = t_{i-1} + \Delta t$, where $\Delta t$ is a step size of the time parameter. An object of initial shape and material properties is loaded by static load which substitutes dynamic load (a real cause of changes [8]). Displacements $u_f$ and stimulus $S$ distribution are calculated for that load, then rates of change in the density and the thickness and finally new values of the thickness and the density are evaluated according to the following relationships:

$$g_i = g_{i-1} + \frac{\mathrm{d}g}{\mathrm{d}t}\Delta t \tag{9}$$

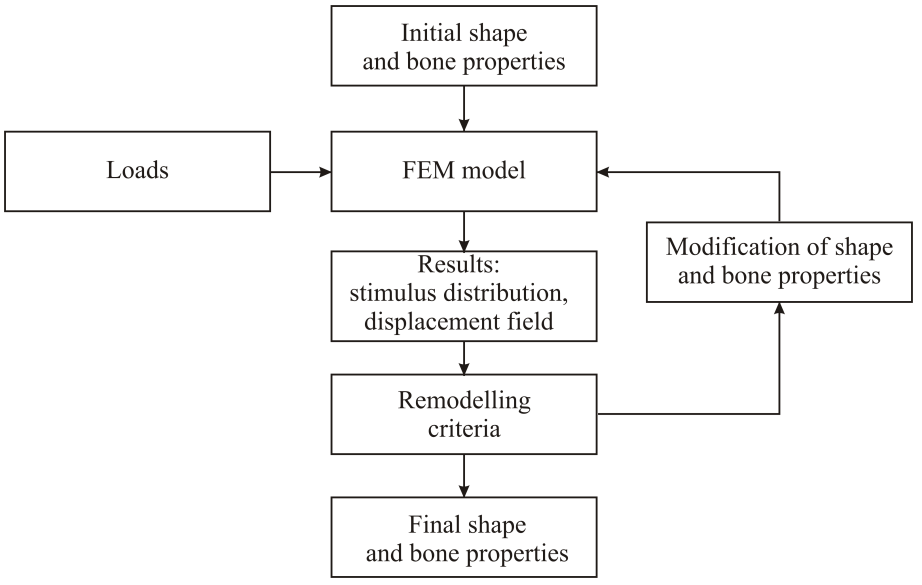


Fig. 3. Block diagram of the remodelling procedure

$$\rho_i = \rho_{i-1} + \frac{\mathrm{d}\rho}{\mathrm{d}t}\Delta t \tag{10}$$

where: $g_i$ – new value of thickness for $i$-th step, $g_{i-1}$ – value of thickness for step no. $i-1$, $\rho_i$ – new value of density for i-th step, $\rho_{i-1}$ – value of density for step no. $i-1$.

The change of shape („creep-like" behaviour) is implemented according to the formula:

$$\mathbf{X}_i = \mathbf{X}_{i-1} + Be^{-B_1 t}\mathbf{u}_f \tag{11}$$

where: $\mathbf{X}_i$ – new locations of points of bone tissue for $i$-th step, $\mathbf{X}_{i-1}$ – locations of bone tissue for step no. $i-1$, $\mathbf{u}_f$ – displacements caused by the load, $B$, $B_1$ – experimental factors.

All abovementioned calculations are conducted until no significant changes in bone tissue are observed.

### 2.3. Finite element model of spine segment with artificial intervertebral disc

The analyses were performed using the Ansys system. The remodelling procedure was written in the Ansys Parametric Design Language (APDL). Owing to the works conducted by the authors [9, 10], a model of a part of spinal segment with an artificial intervertebral disc was used to investigate remodelling of the bone. The model includes a part of the vertebra and upper plate of the prosthesis (Fig. 4). The spinal segment was considered to be symmetrical with respect to the sagittal plane, so only its right part was analysed with appropriate boundary conditions.

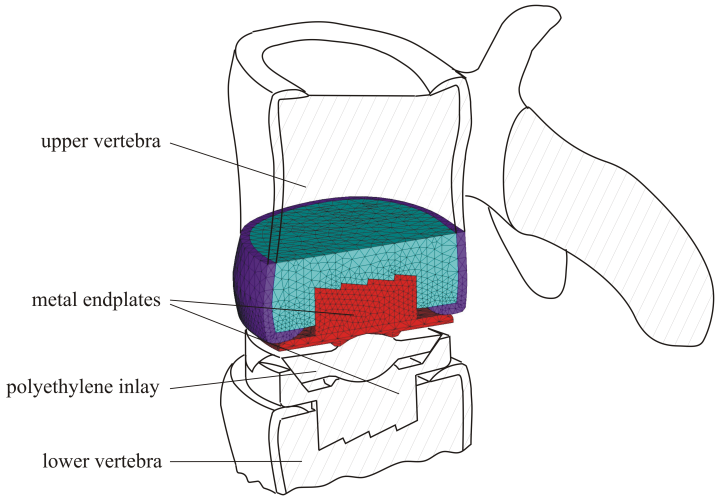


Fig. 4. Finite element model of the fragment of the vertebra with artificial intervertebral disc (sagittal plane section)

The dimensions of the model of the vertebra were: depth 36mm, width 54mm, height 37mm. Isotropy of all used materials was assumed (Table 1). The parameters $\alpha$ and $\beta$ which describe relation between apparent density and Young's moduli of bone tissue (1) were assumed 4 249 and 3, respectively. The model consisted of 4 5697 elements of 10 213 nodes.

Table 1.

Initial Young's moduli ($E$), Poisson's ratio values ($\nu$), thicknesses ($\delta$) and densities ($\rho$)

| | $E$ [N/mm$^2$] | $\nu$ | $\rho$ [g/cm$^3$] | $\delta$ [mm] |
|---|---|---|---|---|
| Cortical bone | 12000 | 0.3 | 1.414 | 1.5 |
| Trabecular bone | 100 | 0.4 | 0.287 | – |
| Endplates of the prosthesis | 200000 | 0.3 | unimportant in the analysis | – |

The cortical bone was modelled with triangle shell elements SHELL63, the trabecular bone end the artificial intervertebral disc were modelled with tetrahedron volume elements SOLID45. There are contact elements CONTA174 and TARGET170 between the endplate of the disc and the vertebrae, whereas the keel and the teeth of the prosthesis are bonded with the vertebra. The plate of the prosthesis is fixed at the surface adjacent to the polyethylene inlay. This condition differs from reality, but according to the de Saint Venant principle it influences results in close vicinity of the support only, and does not change the stress distribution within the bone. The model was loaded by vertical displacement ($z$ component, Fig. 5) of its upper surface, so that the net vertical force was 3000 N. The same value of the displacement was assigned to all nodes of the surfaces, but due to the changes in

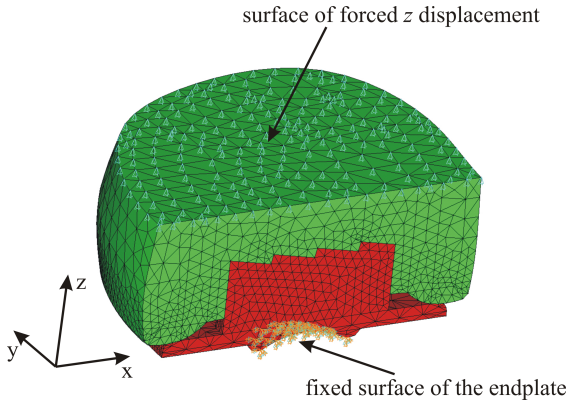


Fig. 5. Finite element mesh of the model with loads. Blue triangles are symbols of displacement applied

stiffness of the system caused by the remodelling, it was not constant over time and was a result of iterative procedure.

Lower and upper limits of density value were assumed, respectively, $\rho_{\min} = 0.005$ [g/cm$^3$] and $\rho_{\max} = 2$ [g/cm$^3$].

Two variants of stimulus formulation (e.g. site-independent and site-dependent) were considered. In the former one, reference stimulus ($S_0$) values were taken from the analysis of intact vertebra, whereas in the latter one the average value of the stimulus for vertebra after prosthesis implantation was assumed as a reference value. Table 2 shows values of parameters used in the remodelling simulations. 14 characteristic points and 26 dimensions were chosen to better observe changes in the shape of the bone (Fig. 6, Table 3).

Table 2.

Bone remodelling process steering parameters (for trabecular bone in brackets)

| Simulation formulation | site independent | site dependent |
|---|---|---|
| $\Delta t$ | 0,01 | 0,01 |
| $C$ ($C_g$) | 50 (5) | 2.5 ($2.5 \cdot 10^{-4}$) |
| $C_1$ ($C_{1g}$) | 25 (25) | 25 (50) |
| $A$ | 250 | 5 |
| $A_1$ | 25 | 25 |
| $B$ | 3 | 3 |
| $B_1$ | 50 | 50 |
| $S_0$ ($S_{0g}$) [J/g] | 0.0105 ($2.48 \cdot 10^{-2}$) | function of location |
| $s$ ($s_g$) | 0.905 (0.9) | 0.35 (0.35) |
| $S_d$ ($S_{dg}$) [J/g] | $1 \cdot 10^{-4}$ | $0.01S_0$ |
| $S_g$ ($S_{gg}$) [J/g] | 0.1 (0.5) | $10S_0$ ($10S_{0g}$) |

Table 3.

Initial distances between characteristic points

| Initial distances [mm] | | | |
|---|---|---|---|
| **L3** | 34.007 | **h1** | 11.833 |
| **L4** | 1.850 | **h2** | 12.333 |
| **L5** | 6.149 | **h3** | 12.505 |
| **L6** | 8.350 | **h4** | 10.833 |
| **L7** | 7.850 | **h5** | 4.833 |
| **L8** | 8.070 | **h6** | 10.833 |
| **L9** | 8.437 | **h7** | 12.505 |
| **L10** | 8.350 | **h8** | 12.333 |
| **L11** | 7.850 | **h9** | 11.833 |
| **L12** | 6.149 | **h10 (points 7 and A)** | 0.500 |
| **L13** | 1.850 | **h11 (points 8 and A)** | 0.000 |
| | | **h12 (points 11 and A)** | −0.172 |
| | | **h13 (points 9 and A)** | 0.500 |
| | | **h14 (points 10 and A)** | 0.000 |
| | | **h15 (points 12 and A)** | −0.172 |

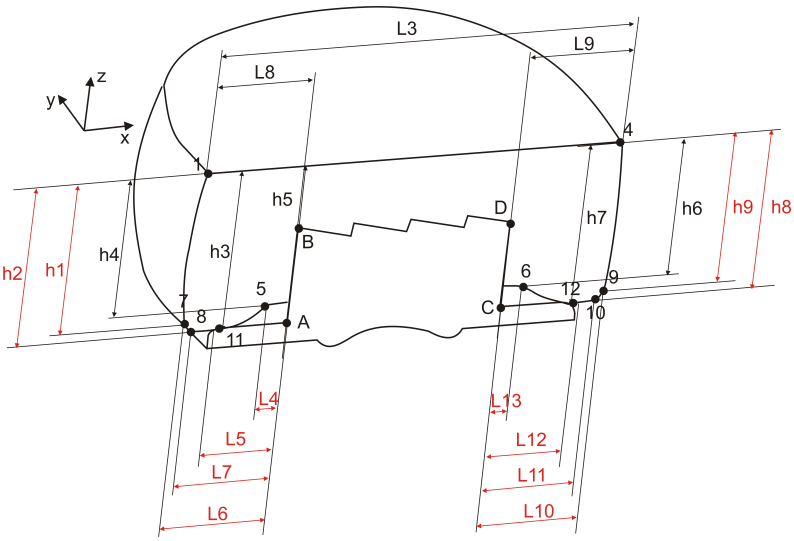


Fig. 6. Characteristic points and dimensions of the model

## 3. Results

The obtained results show that stimuli defined in different ways (site-independent and site-dependent) give qualitatively different bone remodelling patterns. Relatively, the least dissimilarities are for cortical bone thickness. Both site-dependent

and site-independent definitions result in changes in thickness observed at ventral and dorsal parts of the endplates (Fig. 7, Table 4). Noticeable differences are:

- more extensive thickness increase zone at ventral part of the endplate for the site-independent stimulus,
- thickness decrease zone at ventral part of side surface of the vertebra for the site-dependent stimulus.

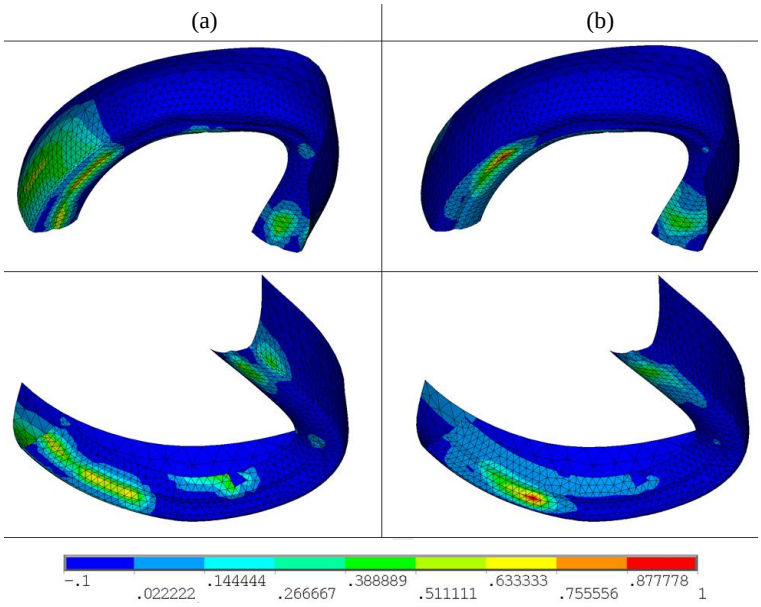


Fig. 7. Cortical bone thickness changes for site-independent (a) and site-dependent (b) stimuli. Value 0 depicts no changes and 1 depicts maximal observed increase of thickness

Table 4.

Final thickness values of the cortical bone

| Stimulus formulation | Thickness [mm] (relative change of thickness [%]) | |
|---|---|---|
| | decrease | increase |
| site-independent | 1.494 (−0.4) | 1.752 (16.8) |
| site-dependent | 1.363 (−9.1) | 2.835 (89.0) |

More differences are visible in the case of bone density changes, especially for the trabecular bone (Fig. 8, Table 5). For the site-dependent stimulus, the changes are observed in the whole vertebra, whereas for the site independent stimulus – in the surrounding of the keel of the prosthesis only. There is a domination of density increase in terms of values and volume affected for the site-dependent stimulus and domination of density increase in terms of volume but density decrease in terms of values for the site-independent stimulus.

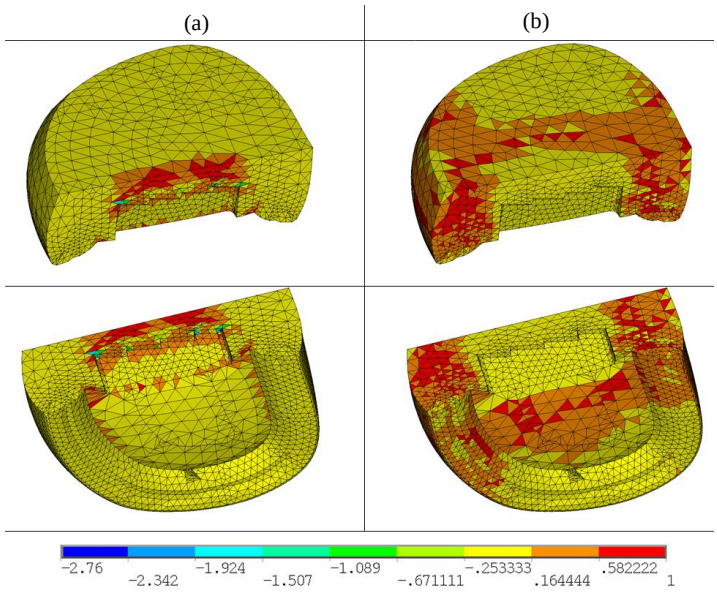


Fig. 8. Trabecular bone density changes for site-independent (a) and site-dependent (b) stimuli. Value 0 depicts no changes and 1 depicts maximal observed increase of density

Table 5.

Final density values of the trabecular bone

| Stimulus | Density [g/cm$^3$] (relative change of density [%]) | |
|---|---|---|
| formulation | decrease | increase |
| site-independent | 0.0005 (−99.8) | 0.390 (35.9) |
| site-dependent | 0.113 (−60,6) | 0.812 (182.9) |

For a cortical bone, the dissimilarities between models are not so high, but still they are not negligible (Fig. 9, Table 6). There is a punch-like (at the ventral part of the endplate) decrease in density for the site-independent variant and a

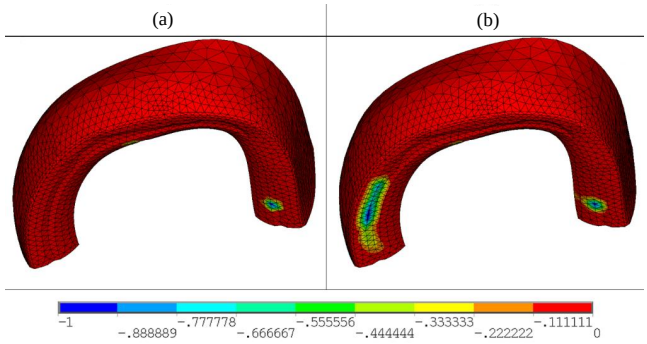


Fig. 9. Cortical bone density changes for site independent (a) and site dependent (b) stimuli. Value 0 depicts no changes and −1 depicts maximal observed decrease of the density

Table 6.

Final density values of the cortical bone

| Stimulus | Density [g/cm$^3$] (relative change of density [%]) | |
|---|---|---|
| formulation | decrease | increase |
| site-independent | 1.406 (−0.6) | 1414 (0) |
| site-dependent | 1.412 (−0.14) | 1.414 (0) |

more widespread one (at both dorsal and ventral parts of the endplate) for the site-dependent variant.

The only mechanism of remodelling whose effects are not directly dependant on the stimulus value (and neither on the definition of the stimulus) is the creep-like mechanism (Fig. 10, Table 7). The differences between permanent deformations, which are visible for site-independent and site-dependent stimuli models, are a result of different density and thickness distributions thus different stiffness of the bone tissue.

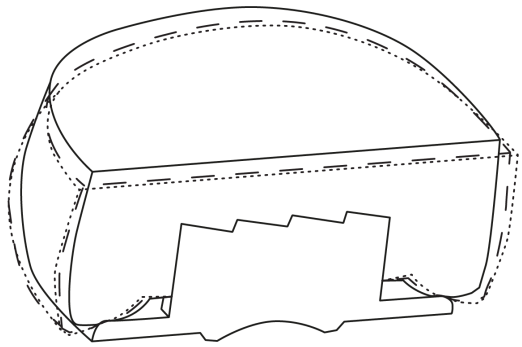

Fig. 10. Changes of shape of the vertebra for site independent (the dotted line) and site dependent (the dashed line) stimuli (the black line – initial shape)

Table 7.

Changes in characteristic dimensions

| Δh1 [mm] | Δh2 [mm] | Δh4 [mm] | Δh8 [mm] | Δh9 [mm] | ΔL5 [mm] | ΔL6 [mm] | ΔL7 [mm] | ΔL10 [mm] | ΔL11 [mm] | ΔL12 [mm] | ΔL13 [mm] |
|---|---|---|---|---|---|---|---|---|---|---|---|
| Stimulus site independent | | | | | | | | | | | |
| −0.423 | −0.595 | −1.903 | −0.553 | −0.357 | 0.425 | 0.522 | 0.398 | 0.526 | 0.379 | 0.393 | 0.765 |
| Stimulus site dependent | | | | | | | | | | | |
| −0.326 | −0.443 | −1.211 | −0.395 | −0.256 | 0.313 | 0.402 | 0.311 | 0.405 | 0.292 | 0.286 | 0.422 |

## 4. Discussion

Unfortunately, the authors were not able to find enough data to make a comprehensive comparison between the numerical results and clinical observations. The problem applies mainly to bone density and thickness distribution. The discrepancy between the results for both definitions of the stimulus may indicate that only one of them is close to the reality. To assess which one fulfils this condition, one needs to carry out further investigation of the clinical outcomes.

Simulations of the change in shape of the vertebrae may be found in the literature [11–13]. However, results of these authors cannot be compared with the results of the current work, because they do not apply to the changes associated with implantation. They show only that healthy vertebra's shape is optimal in a way.

According to [14], intervertebral disc degeneration leads to an increase in trabecular bone density in non-central part of the vertebra. Paper [15] proves that implantation of an artificial disc gives stress patterns similar to those caused by the degenerated disc [16], so it can even deepen this effect. The results of the proposed model for the site-dependent stimulator (Fig. 8b) feature similar tendency. A difference is that the initial density distribution in [14] is nonuniform and becomes more uniform, whereas in the present paper there is an opposite situation.

There is more information on permanent deformation of the vertebral body. The subsidence, which is a result of numerical simulation (Fig. 11), coincides with the response of the real bone presented in several papers [17–20]. This fact supports employment of the so-called "creep-like" behaviour component into the remodelling model. It is worth noting that a mechanism of similar nature (mechanically induced displacements became permanent) was recently included in a model proposed by Wrona on trabeculae level [21].

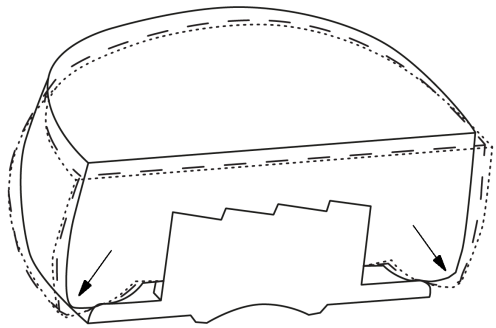

Fig. 11. Subsidence of the implant obtained in the numerical simulation

In the simulations, one assumed uniform initial distribution of density and thickness. It seems that this condition should be improved in further works. This may refer mainly to the cortical bone. As a matter of fact, [12] indicates that

cancellous bone density is higher in the central region of vertebra but, as it was mentioned earlier [14], the degenerated disc, which is later substituted with the artificial one, causes more uniform density distribution.

Also, the assumed isotropy of the bone material used in the simulation may raise doubts (although it still exists in literature e.g. [22]) and should be revised, but this requires modification of the model and the used procedures, which was considered purposeless at the initial stage of the work.

Manuscript received by Editorial Board, July 07, 2016;
final version, October 04, 2016.

## References

[1] T. Lekszycki. Optimality conditions in modeling of bone adaptation phenomenon. *Journal of Theoretical and Applied Mechanics*, 37(3): 607-623, 1999.

[2] G. Krzesiński. *Numerical simulation methods in stress analysis of bone tissue and implant design*. Oficyna Wydawnicza Politechniki Warszawskiej, 2012. (in Polish).

[3] J.J. Telega and T. Lekszycki. Reconstruction of bone tissue: the evolution of concepts and models. In R. Będziński, K. Kędzior, J. Kiwerski, A. Morecki, K. Skalski, A. Wall, A. Witt, editors *Biomechanics and Rehabilitation Engineering*, volume 5, EXIT, Warsaw, 2004. (in Polish).

[4] A. Dąbrowska-Tkaczyk and M. Pawlikowski. Influence of remodelling stimulating factor selection on bone density distribution in pelvic bone model. *Acta of Bioengineering and Biomechanics*, 8(2):119-126, 2006.

[5] M. Nowak. On some properties of bone functional adaptation phenomenon useful in mechanical design. *Acta of Bioengineering and Biomechanics*, 12(2):49-54, 2010.

[6] K. Tsubota, T. Adachi and Y. Tomita. Functional adaptation of cancellous bone in human proximal femur predicted by trabecular surface remodelling simulation toward uniform stress state *Journal of Biomechanics*, 35(12):1541-1551, 2002.

[7] M. Reicher and A. Bochenek. *Human Anatomy*. volume 1, Wydawnictwo Lekarskie PZWL, 1990. (in Polish).

[8] R. Huiskes. If bone is the answer, then what is the question?. *Jouranl of Anatomy*, 197(2):145-156, 2000.

[9] P. Borkowski, K. Kędzior, G. Krzesiński, K.R. Skalski, P. Wymysłowski and T. Zagrajek. Numerical investigation of a new type of artificial lumbar disc. *Journal of Theoretical and Applied Mechanics*, 42(2):253-268, 2004.

[10] P. Borkowski, P. Marek, G. Krzesiński, J. Ryszkowska, B. Waśniewski, P. Wymysłowski and T. Zagrajek. Finite element analysis of artificial disc with an elastomeric core in the lumbar spine. *Acta of Bioengineering and Biomechanics*, 14(1):59-66, 2012.

[11] V.K. Goel, S.A. Ramirez, W. Kong and L.G. Gilbertson. Cancellous bone Young's modulus variation within the vertebral body of a ligamentous lumbar spine – application of bone adaptive remodelling concepts. *Journal of Biomechanical Engineering*, 117(3):266-271, 1995.

[12] X. Wang and G.A. Dumas. Simulation of bone adaptive remodeling using stochastic process as loading history. *Journal of Biomechanics*, 35(3):375-380, 2002.

[13] Zhu Xinghua, Gong He, Zhu Dong, Gao Bingzhao, A study of the effect of non-linearities in the equation of bone remodeling. *Journal of Biomechanics*, 35(7):951-960, 2002.

[14] X. Wang and G.A. Dumas. Evaluation of effects of selected factors on inter-vertebral fusion – a simulation study. *Medical Engineering & Physics*, 27(3):197-207, 2005.

[15] V. Palissery, R.C. Mulholland and D.S. McNally. The implications of stress patterns in the vertebral body under axial support of an artificial implant. *Medical Engineering & Physics*, 31(7):833-837, 2009.
[16] J. Homminga, R. Aquarius, V.E. Bulsink, C. Jansen and N. Verdonschot. Can vertebra density changes be explained by intervertebral disc degeneration? *Medical Engineering & Physics*, 34(4):453-458, 2012.
[17] B.W. Cunningham, G.L. Lowery, H.A. Serhan, A.E. Dmitriev, C.M. Orbegoso, P.C. McAfee, R.D. Fraser, R.E. Ross and S.S. Kulkarni. Total disc replacement arthroplasty using the AcroFlex lumbar disc: a non-human primate model. *European Spine Journal*, 11:S115-S123, 2002.
[18] W.B. Cunningham. Basic scientific considerations in total disc arthroplasty. *The Spine Journal*, Suppl. 4(6):S219-S230, 2004.
[19] B.J.C. Freeman and J. Davenport. Total disc replacement in the lumbar spine: a systematic review of the literature. *European Spine Journal*, 15: 439-447, 2006.
[20] H.D. Link. History, design and biomechanics of the LINK SB Charité artificial disc. *European Spine Journal*, 11:S98-S105, 2002.
[21] A. Wrona. Computer algorithm for examination of the remodelling process in the cancellous bone. *Acta Bio-Optica et Informatica Medica. Inżynieria Biomedyczna*, 20(1):1–10, 2014. (in Polish).
[22] W. Wolański and D. Larysz D. *Biomechanics of stabilizing the cervical spine*. BEL Studio, 2011. (in Polish).

**Model przebudowy kości uwzględniający zmiany struktury i kształtu spowodowane trzema różnymi mechanizmami przebudowy. Przypadek kręgosłupa lędźwiowego**

Streszczenie

Artykuł prezentuje metodę analizy przebudowy kości w otoczeniu implantów. Celem pracy było opracowanie modelu i procedur numerycznych mogących służyć jako narzędzie wspomagające projektowanie protez. Zaproponowany przez autorów model opiera się na teorii adaptacyjnej sprężystości i koncepcji strefy martwej. Uwzględnia on nie tylko zmiany struktury wewnętrznej tkanki (opisanej przez gęstość pozorną), ale także przebudowę powierzchniową i zmiany związane z efektami wykazującymi pewne cechy "pełzania". Przeprowadzona została analiza metodą elementów skończonych segmentu ruchowego kręgosłupa ze sztucznym krążkiem międzykręgowym z wykorzystaniem systemu Ansys i własnego kodu APDL. Algorytmy zbudowano w dwóch wariantach: tzw. niezależnym i zależnym od miejsca. Porównano uzyskane rozkłady gęstości i zmiany kształtu pokazując, że obydwa warianty przebudowę kości przewidują w różny sposób. Zaprezentowano również porównanie wyników numerycznych z badaniami klinicznymi wskazując na ich podobieństwa.